



Original Article



Insights about cervical lymph nodes: Evaluating deep learning–based reconstruction for head and neck computed tomography scan

Yu-Han Lin^a, An-Chi Su^a, Shu-Hang Ng^a, Min-Ru Shen^b, Yu-Jie Wu^c, Ai-Chi Chen^d, Chia-Wei Lee^d, Yu-Chun Lin^{a,e,*}

^a Department of Medical Imaging and Intervention, Chang Gung Memorial Hospital, Taoyuan, Taiwan

^b Department of Diagnostic Radiology, Chang Gung Memorial Hospital, Keelung, Taiwan

^c Department of Radiology, Shuang Ho Hospital, Taipei Medical University, New Taipei City, Taiwan

^d General Electric (GE) Healthcare, Taiwan

^e Department of Medical Imaging and Radiological Sciences, Chang Gung University, Taoyuan, Taiwan

ARTICLE INFO

Keywords:

Lymph nodes
Head and neck neoplasms
Image processing
Computer-assisted
Multidetector computed tomography
Deep learning
Image enhancement

ABSTRACT

Purpose: This study aimed to investigate differences in cervical lymph node image quality on dual-energy computed tomography (CT) scan with datasets reconstructed using filter back projection (FBP), hybrid iterative reconstruction (IR), and deep learning–based image reconstruction (DLIR) in patients with head and neck cancer.

Method: Seventy patients with head and neck cancer underwent follow-up contrast-enhanced dual-energy CT examinations. All datasets were reconstructed using FBP, hybrid IR with 30 % adaptive statistical IR (ASiR-V), and DLIR with three selectable levels (low, medium, and high) at 2.5- and 0.625-mm slice thicknesses. Herein, signal, image noise, signal-to-noise ratio, and contrast-to-noise ratio of lymph nodes and overall image quality, artifact, and noise of selected regions of interest were evaluated by two radiologists. Next, cervical lymph node sharpness was evaluated using full width at half maximum.

Results: DLIR exhibited significantly reduced noise, ranging from 3.8 % to 35.9 % with improved signal-to-noise ratio (11.5–105.6 %) and contrast-to-noise ratio (10.5–107.5 %) compared with FBP and ASiR-V, for cervical lymph nodes ($p < 0.001$). Further, 0.625-mm-thick images reconstructed using DLIR-medium and DLIR-high had a lower noise than 2.5-mm-thick images reconstructed using FBP and ASiR-V. The lymph node margins and vessels on DLIR-medium and DLIR-high were sharper than those on FBP and ASiR-V ($p < 0.05$). Both readers agreed that DLIR had a better image quality than the conventional reconstruction algorithms.

Conclusion: DLIR-medium and -high provided superior cervical lymph node image quality in head and neck CT. Improved image quality affords thin-slice DLIR images for dose-reduction protocols in the future.

1. Introduction

In patients with head and neck cancer, computed tomography (CT) is the common first-line standard imaging for evaluating primary tumors and regional lymph nodes. Sufficient image quality and spatial resolution are essential for diagnosing different conditions, particularly lymphadenopathy. Meanwhile, misclassifying lymph nodes before

treatment may lead to poor prognosis. CT plays an important role in providing morphological information on the characteristics of lymph nodes (such as shape, size, and pattern on contrast enhancement) [1]. Generally, metastasis is defined as lymph nodes with a short axis (>10 mm) [1]. Some studies have reported that nodal size measurement, particularly in small-sized lesions, may be reader-dependent due to irregular or poorly defined margins [2]. Thus, imaging with a high

* Correspondence to: Department of Medical Imaging and Intervention, Chang Gung Memorial Hospital, Linkou, No.5, Fuxing St., Guishan Dist., Taoyuan City 333, Taiwan.

E-mail address: jack805@cgmh.org.tw (Y.-C. Lin).

<https://doi.org/10.1016/j.ejro.2023.100534>

Received 16 May 2023; Received in revised form 14 October 2023; Accepted 20 October 2023

Available online 28 October 2023

2352-0477/© 2023 The Authors. Published by Elsevier Ltd. This is an open access article under the CC BY-NC-ND license (<http://creativecommons.org/licenses/by-nc-nd/4.0/>).

spatial resolution is helpful to determine the risk of nodal metastasis. In conventional CT, assessing metastasis to normal-sized lymph nodes with subtle intranodal necrosis or extracapsular spread remains challenging. A better visualization of lymph nodes may increase diagnostic accuracy for treatment decision-making.

Filtered back projection (FBP) is an algorithm used in conventional image reconstruction (conversion from the measured data to the image) on CT scanners. FBP is a fast and direct method for generating CT images [3]. By contrast, hybrid model-based adaptive statistical iterative reconstruction (ASiR-V) [4], which uses a more complex system of prediction models, is an algorithm utilized in iterative reconstruction (IR) and can reduce image noise and improve image quality compared with FBP [5,6]. Currently, the deep learning technology has an excellent performance in various fields of medical imaging. A commercial deep learning-based image reconstruction (DLIR) algorithm has been recently utilized in image noise reduction on CT [7]. DLIR can deal with complex models and large parameters via training processes. This post-processing technique can improve the quality of CT images, thereby leading to significant progress in most clinical situations, particularly when performing high-resolution CT imaging.

DLIR outperforms FBP and IR techniques in terms of CT image quality in different fields, particularly the chest and abdominal regions [8–10]. However, it has not been previously applied on cervical lymph node CT in patients with head and neck cancer. Thus, this study aimed to investigate differences in the image quality of cervical lymph nodes on

CT with datasets reconstructed using FBP, ASiR-V, and DLIR in patients with head and neck cancer. It primarily aimed to identify the reconstruction method with the best image quality.

2. Materials and methods

2.1. Study design and population

This retrospective study was approved by the Research Ethics Committee of *BLINDED* (approval number: 2019019900B0). The requirement for informed consent was waived owing to the retrospective design of this study. Fig. 1 shows the diagram of the study design. There were 70 post-treatment patients aged 38–81 years with histologically confirmed head and neck cancer. Among them, 63 were men and 7 women (mean ± standard deviation: 56.4 ± 10.4 years). The patients underwent contrast-enhanced standard-of-care follow-up CT study between June 2021 and August 2021. The datasets of contrast-enhanced head and neck CT were evaluated with the dual-energy protocol using a 256-multidetector CT scanner (Revolution CT, *BLINDED*) at a standard dose.

Images were acquired 60 s after injecting 100 mL of contrast agent intravenously (Omnipaque 350 mg/mL; iohexol, *BLINDED*) at a rate of 2.5 mL/s. The main scanning parameters were as follows: tube voltage, 80–140 kVp; noise index, 9; gantry rotation time, 0.5 s; detector collimation, 40 × 0.625 mm; pitch factor, 0.984:1; and matrix,

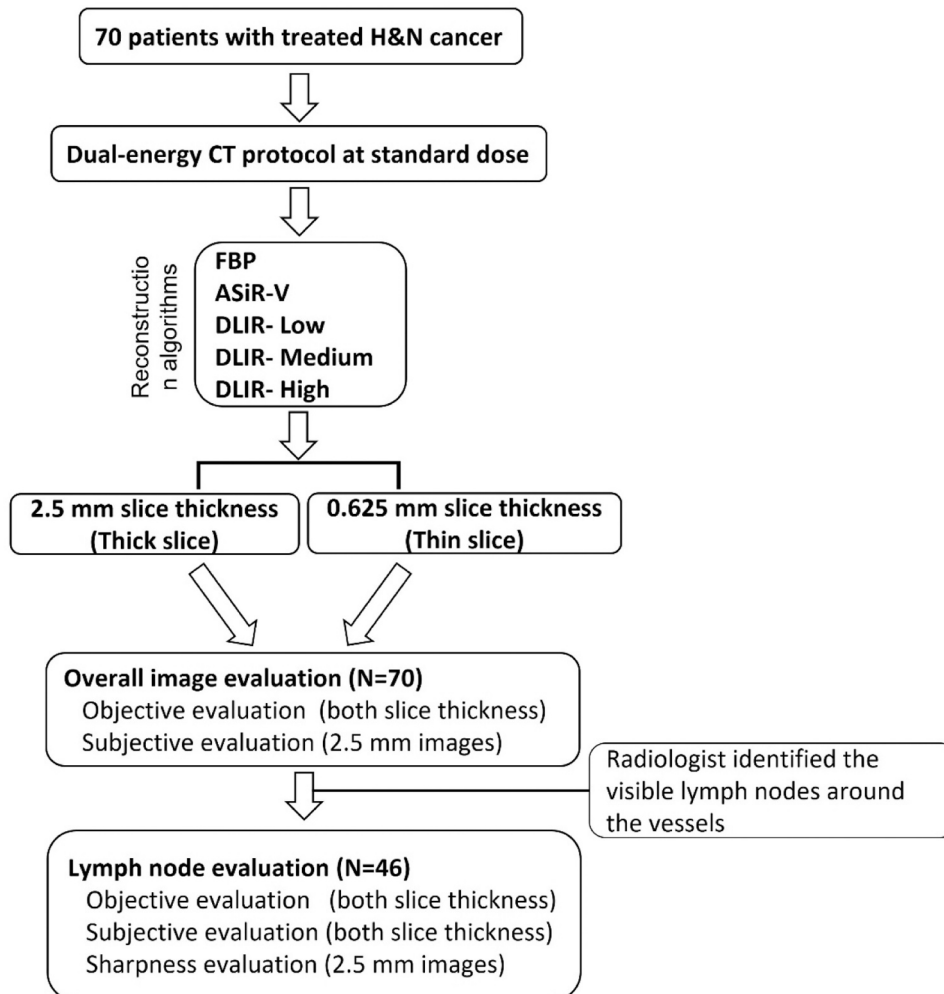


Fig. 1. Flow chart of the study design.

512 × 512 with auto current modulation. The data of each patient were reconstructed with 120-kVp-like images at both 2.5-mm (thick) and 0.625-mm (thin) slice thickness with the FBP, ASiR-V, and DLIR algorithms (TrueFidelity, *BLINDED*). ASiR-V was reconstructed at a blending level of 30 % ASiR-V. DLIR was reconstructed with three strength levels (low, medium, and high). Metal artifact reduction was used if implants were installed. In addition to evaluating thick-slice images, the overall image quality of the cervical lymph nodes was assessed using thin-slice images that simulated dose-reduction protocols with higher noise levels.

2.2. Assessment of overall image quality

To compare image quality, the signal (mean attenuation value), noise, signal-to-noise ratio (SNR), and contrast-to-noise ratio (CNR) in all datasets were evaluated. Circular regions of interest (ROI) measuring 20 mm² were placed on the masseter muscle, sternocleidomastoid muscle, internal jugular vein, submandibular gland, and fat as background using an advanced workstation (AW 4.7, *BLINDED*). CT number and standard deviation represent the mean attenuation value (HU) and noise (SD) of each ROI. SNR and CNR were calculated using the following formula (1–2):

$$SNR = \frac{\text{average of } ROI_{LV}}{\text{standard deviation of } ROI_{fat}} \quad (1)$$

$$CNR = \frac{\text{average of } ROI_{LV} - \text{average of } ROI_{fat}}{\text{standard deviation of } ROI_{fat}} \quad (2)$$

Two radiologists, one with 27 years of experience in head and neck imaging and the other with 4 years of experience as a resident, assessed all images reconstructed at 2.5-mm slice thickness. Both were blinded to patient information and reconstruction types, and they independently evaluated images in random order with fixed window widths and levels of 350 and 50 Hounsfield Units (HU), respectively. The overall image quality and noise were rated with a five-point scale (5 = excellent quality/minimal noise, 4 = better quality for diagnosis/less than average noise, 3 = average quality/acceptable noise, 2 = suboptimal quality/above than average noise, and 1 = poor quality/unacceptable noise). Meanwhile, the artifact was graded with a three-point scale (3 = no artifact/excellent visualization, 2 = minor artifact/acceptable for diagnosis, and 1 = major artifact/unacceptable for diagnosis).

2.3. Image quality evaluation of the lymph node region

In total, 46 lymph nodes (29 normal and 17 malignant lymph nodes) around the vessels at different neck levels were identified by the radiologist with 6 years of experience, and a circular ROI was placed at its largest diameter section on 2.5- and 0.625-mm images. Objective and subjective analyses were performed to investigate the lymph nodes. In addition, the noise reduction rate and differences in SNR and CNR were calculated between DLIR and both FBP and ASiR-V. The equations were as follows (3–5):

$$\text{Noise reduction rate (\%)} = \frac{N_{DLIR(L,M,H)} - N_{FBP,ASiR}}{N_{FBP,ASiR}} \times 100 \quad (3)$$

$$\text{Differences of SNR (\%)} = \frac{SNR_{DLIR(L,M,H)} - SNR_{FBP,ASiR}}{SNR_{FBP,ASiR}} \times 100 \quad (4)$$

$$\text{Differences of CNR (\%)} = \frac{CNR_{DLIR(L,M,H)} - CNR_{FBP,ASiR}}{CNR_{FBP,ASiR}} \times 100 \quad (5)$$

The sharpness of lymph nodes on 2.5-mm images was evaluated via histogram analysis with full width at half maximum (FWHM). One three-Gaussians kernel was used to fit the distribution of selected ROIs, including the lymph nodes, arterial, and venous regions in each. The FWHM values of each region were used to assess the sharpness of images

via DL and non-DL reconstructions. In addition, the two readers rated the sharpness and noise of lymph nodes on 2.5- and 0.625-mm slice-thickness images with a five-point scale (5 = sharpest/minimal noise, 4 = better than average/less than average noise, 3 = average/acceptable noise, 2 = suboptimal/acceptable for diagnosis, and 1 = blurry/unacceptable for diagnosis).

2.4. Statistical analysis

Data were presented as mean ± standard deviation and were analyzed using GraphPad Prism 5 (GraphPad Prism Software). The figures in this study were expressed using both bar charts, which showed the mean and standard error of the mean, and box plots, which depicted the mean and standard deviation. Within all tables, the values were displayed as mean along with standard deviation. A p-value of 0.05 was considered statistically significant. To compare reconstructions in terms of objective image quality, repeated-measures analysis of variance was used, followed by the post-hoc Tukey's test for multiple comparisons. The paired *t*-tests were utilized to compare differences between DLIR at all strength levels and the two conventional reconstruction algorithms. All datasets were tested for linearity using the Shapiro–Wilk test. Subjective analysis within readers across reconstructions was performed using the Likert scale and the Kruskal–Wallis test. We investigated the intraclass correlation coefficient (ICC) to investigate the agreement between readers.

3. Results

3.1. Objective evaluation of the overall image quality

Fig. 2 shows the head and neck CT images reconstructed with different algorithms at 2.5- and 0.625-mm slice thicknesses. The lymph node is highlighted with an arrow. Based on the images, DLIR was superior to the conventional reconstruction algorithms in terms of image quality, noise, and sharpness. Table 1 depicts the objective analysis results. In particular, on the 2.5-mm image, only the signal of the sternocleidomastoid muscle and submandibular gland was significantly higher in DLIR-high (H) than in FBP (*p* = 0.008 and 0.028, respectively) (Supplementary Table 1). On the 0.625-mm image, the sternocleidomastoid muscle and masseter muscle had a higher signal in DLIR-H than in FBP and ASiR-V (*p* < 0.001). DLIR had a significantly higher noise reduction than the two reconstruction methods (*p* < 0.001) across all ROIs and slice thicknesses (Supplementary Table 2). In addition, DLIR had a better SNR and CNR (*p* < 0.001), with DLIR at the highest strength outperforming all other reconstructions in terms of SNR and CNR, followed by ASiR-V and FBP at medium and low strengths (Table 1). Notably, despite higher noise levels, 0.625-mm images from DLIR-M and DLIR-H had a lower noise than 2.5-mm images from FBP and ASiR-V.

3.2. Subjective evaluation of the overall image quality

Table 2 shows the subjective scores of image quality, noise, and artifacts from the two readers. Both agreed that images reconstructed using DLIR had a better image quality than those reconstructed using ASiR-V and FBP (*p* < 0.001). In particular, DLIR-medium (M) had the best image quality score from one reader. Meanwhile, the other reader assigned the highest score to DLIR-H. With the metal artifact reduction technique, DLIR had significantly less artifacts (*p* < 0.05 and 0.001 for both readers). DLIR-H had the best noise score, followed by ASiR-V and FBP at medium and low strengths (*p* < 0.001). The ICCs for image noise, artifact, and image quality were 0.79 (95 % confidence interval [CI]: 0.74–0.82), 0.31 (95 % CI: 0.21–0.4), and 0.48 (95 % CI: 0.38–0.56) (*p* < 0.001), respectively.

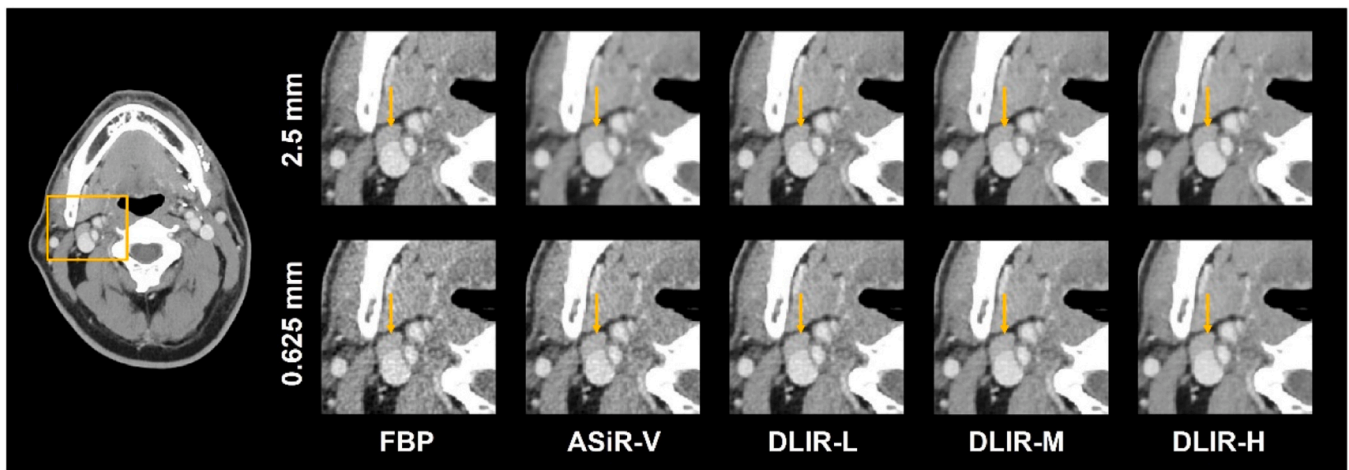


Fig. 2. Images reconstructed with each algorithm at 2.5-mm (upper row) and 0.625-mm (lower row) slice thickness. The lymph node is pointed with a yellow arrow.

Table 1

Overall image quality. SNR and CNR of each ROI at 2.5- and 0.625-mm slice thicknesses using different reconstruction algorithms.

	FBP	ASiR-V	DLIR-L	DLIR-M	DLIR-H	p-value
Thick slice (2.5 mm)						
SNR _{SCM}	8.0 (1.9)	9.9 (2.6)	11.3 (2.9)	12.9 (3.6)	15.2 (14.8)	<0.0001*
SNR _{MM}	5.8 (1.8)	7.1 (2.5)	8.0 (2.8)	9.0 (3.4)	10.4 (4.2)	<0.0001*
SNR _{LJV}	20.5 (7.2)	24.9 (9.3)	27.2 (10.1)	30.6 (11.8)	35.4 (14.6)	<0.0001*
SNR _{SM gland}	8.6 (4.0)	10.4 (5.3)	11.4 (6.0)	12.7 (7.1)	14.3 (8.5)	<0.0001*
SNR _{Fat}	9.1 (2.5)	11.1 (3.3)	12.2 (3.7)	13.6 (4.4)	15.8 (5.4)	<0.0001*
CNR	32.3 (10.4)	39.3 (12.0)	43.2 (14.2)	48.4 (16.7)	55.4 (19.2)	<0.0001*
Thin slice (0.625 mm)						
SNR _{SCM}	5.7 (1.2)	7.0 (1.5)	8.7 (1.9)	10.3 (2.4)	12.9 (3.3)	<0.0001*
SNR _{MM}	4.5 (1.1)	5.5 (1.5)	6.7 (1.8)	7.8 (2.3)	9.4 (3.1)	<0.0001*
SNR _{LJV}	15.2 (4.6)	18.5 (5.8)	22.1 (7.1)	25.8 (8.7)	31.1 (11.2)	<0.0001*
SNR _{SM gland}	7.1 (3.1)	8.6 (2.1)	10.2 (4.8)	11.7 (5.8)	13.7 (7.1)	<0.0001*
SNR _{Fat}	6.8 (1.6)	8.3 (2.1)	10.2 (2.7)	12.1 (3.4)	14.7 (4.6)	<0.0001*
CNR	24.2 (6.6)	29.2 (8.3)	36.0 (10.8)	42.4 (13.2)	51.5 (17.2)	<0.0001*

* Denotes a significant mean difference between each reconstruction algorithm.

3.3. Lymph node evaluation

The image signals of the lymph nodes significantly differed between thin- and thick-slice images ($p < 0.001$) (Table 3). DLIR had the highest noise reduction ($p < 0.001$). According to the post-hoc tests, DLIR-H and DLIR-M had significant noise reduction compared with ASiR-V on 2.5-mm images. However, DLIR-low (L) and ASiR-V had similar noise levels. Images reconstructed using DLIR had a significantly better SNR and CNR (Fig. 3).

DLIR at increasing strengths had higher noise reduction rates (3.8–35.8 %) and SNR and CNR improvements (10.5–73 %) compared with FBP. Hence, DLIR had an effective noise reduction ability (Table 4). Thin-slice images were used to simulate the reduced-dose protocol, which results in higher noise reduction rates, leading to SNR and CNR improvements. According to the two readers, DLIR significantly outperformed ASiR-V and FBP in terms of sharpness and noise ($p < 0.001$)

Table 2

Overall image quality. Subjective score of the overall images using different reconstruction algorithms.

	FBP	ASiR-V	DLIR-L	DLIR-M	DLIR-H	p-value
Reader 1						
Image quality	2.9 (0.8)	3.8 (0.8) ^a	3.9 (0.8) ^a	4.3 (0.5) ^{ab}	4.1 (0.7) ^a	<0.0001
Artifact	2.2 (0.7)	2.3 (0.6)	2.3 (0.7)	2.5 (0.6)	2.6 (0.6) ^a	<0.05
Noise	2.1 (0.5)	2.9 (0.6) ^a	3.4 (0.6) ^{ab}	4.0 (0.4) ^{abc}	4.7 (0.5) ^{abcd}	<0.0001
Reader 2						
Image quality	2.8 (0.5)	2.9 (0.4)	3.5 (0.5) ^{ab}	3.8 (0.5) ^{ab}	4.1 (0.5) ^{abc}	<0.0001
Artifact	1.8 (0.5)	1.9 (0.3)	2.0 (0.5)	2.1 (0.6) ^a	2.3 (0.6) ^{ab}	<0.0001
Noise	2.4 (0.5)	2.9 (0.4)	3.7 (0.5) ^{ab}	4.1 (0.5) ^{ab}	4.9 (0.3) ^{abcd}	<0.0001

^a denotes a significant mean difference compared with FBP.

^b denotes a significant mean difference compared with ASiR-V.

^c denotes a significant mean difference compared with DLIR-L.

^d denotes a significant mean difference compared with DLIR-M.

Table 3

Objective evaluation of the lymph nodes using different reconstruction algorithms.

	FBP	ASiR-V	DLIR-L	DLIR-M	DLIR-H	p-value
Thick slice (2.5 mm)						
SL _{LN}	78.8 (22.9)	78.1 (23.0) ^a	79.4 (22.9) ^{ab}	79.1 (22.9) ^b	78.9 (23.0) ^{bc}	<0.0001
N _{LN}	13.9 (4.3)	12.3 (4.4) ^a	12.1 (4.5) ^a	11.6 (4.6) ^{abc}	11.0 (4.8) ^{abcd}	<0.0001
SNR _{LN}	7.7 (3.0)	9.3 (3.6) ^a	10.3 (4.0) ^{ab}	11.5 (4.6) ^{abc}	13.1 (5.3) ^{abcd}	<0.0001
CNR _{LN}	16.7 (4.6)	20.2 (5.8) ^a	22.3 (6.6) ^{ab}	25.0 (7.8) ^{abc}	28.5 (9.5) ^{abcd}	<0.0001
Thin slice (0.625 mm)						
SL _{LN}	81.1 (23.4)	80.4 (23.4) ^a	80.6 (23.3)	80.3 (23.2) ^a	79.9 (23.3) ^{abc}	<0.0001
N _{LN}	16.8 (4.3)	14.4 (4.2) ^a	13.1 (3.9) ^{ab}	12.0 (4.0) ^{abc}	10.9 (4.1) ^{abcd}	<0.0001
SNR _{LN}	5.9 (2.0)	7.1 (2.5) ^a	8.6 (3.1) ^{ab}	10.1 (3.8) ^{abc}	12.3 (4.8) ^c	<0.0001
CNR _{LN}	12.6 (3.0)	15.2 (3.9) ^a	18.6 (5.0) ^{ab}	21.9 (6.2) ^{abc}	26.6 (8.2) ^{abcd}	<0.0001

^a denotes a significant mean difference compared with FBP.

^b denotes a significant mean difference compared with ASiR-V.

^c denotes a significant mean difference compared with DLIR-L.

^d denotes a significant mean difference compared with DLIR-M.

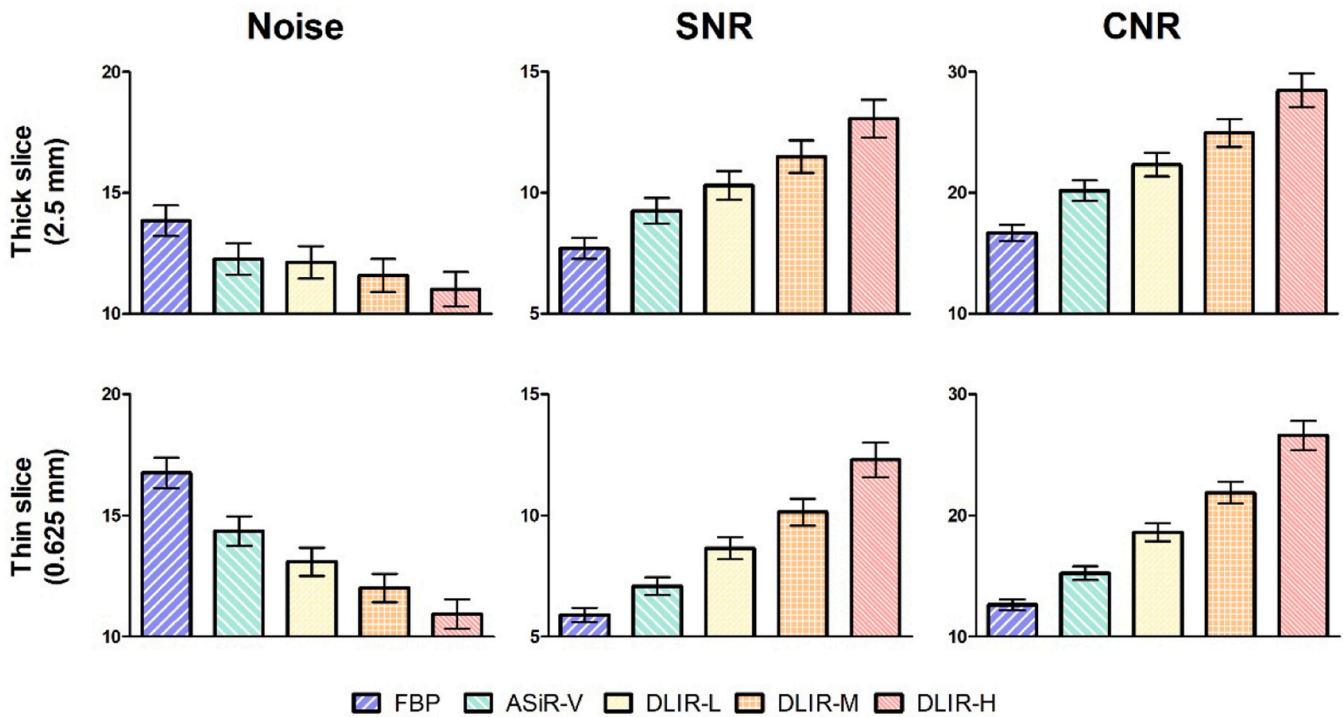


Fig. 3. Lymph node evaluation: noise, SNR, and CNR of the lymph nodes at 2.5-mm (upper row) and 0.625-mm (lower row) slice thickness.

Table 4
Noise reduction rate and differences in SNR and CNR.

		DLIR-L	DLIR-M	DLIR-H
Thick slice (2.5 mm)				
FBP	Noise (%)	14.2 (6.9)	18.6 (9.4)	23.1 (12.7)
	SNR (%)	33.7 (10.1)	49.0 (17.0)	69.5 (27.2)
	CNR (%)	33.4 (10.1)	48.9 (17.1)	69.7 (27.4)
ASiR-V	Noise (%)	3.8 (2.9)	7.3 (5.5)	12.5 (9.6)
	SNR (%)	11.5 (6.1)	24.1 (10.8)	41.0 (18.5)
	CNR (%)	10.5 (6.0)	23.2 (10.8)	40.3 (18.5)
Thin slice (0.625 mm)				
FBP	Noise (%)	22.5 (7.4)	29.1 (10.2)	35.8 (13.0)
	SNR (%)	45.8 (10.5)	70.5 (18.1)	106.2 (32.6)
	CNR (%)	46.4 (10.0)	71.6 (17.4)	108.0 (31.9)
ASiR-V	Noise (%)	9.5 (4.5)	17.4 (7.6)	25.5 (10.9)
	SNR (%)	22.0 (6.8)	42.6 (12.6)	72.3 (24.4)
	CNR (%)	21.9 (6.4)	42.8 (12.1)	73.0 (23.8)

(Fig. 4 and Supplementary Table 3). Superior ICCs for lymph node sharpness are found in thin-slice images (ICC = 0.61, 95 % CI: 0.52–0.68) compared with thick-slice images (ICC = 0.46, 95 % CI: 0.35–0.56, $p < 0.0001$). Additionally, highly correlated ICCs of lymph node noise were observed on both thick and thin-slice images (ICC = 0.75 and 0.73, 95 % CI: 0.68–0.8 and 0.66–0.78, respectively, $p > 0.001$).

Results showed significant differences between DLIR at all strengths and FBP in the lymph nodes and arterial and venous regions ($p < 0.001$) (Fig. 5).

Furthermore, DLIR-L showed no significant difference compared to ASiR-V in cervical lymph nodes, while medium and high strengths exhibited statistically significant improvement ($p < 0.05$). In the arteries, significant differences were observed between all datasets for FBP and ASiR-V ($p < 0.01$). However, in the venous regions, the FWHM of DLIR-L and DLIR-M was similar to that of ASiR-V.

4. Discussion

This study performed the first clinical evaluation of DLIR applied on cervical lymph nodes on head and neck CT study based on the standard-dose protocol. DLIR outperformed ASiR-V and FBP in terms of overall image quality, as evidenced by significant improvement in objective and subjective outcomes. DLIR is a newly developed deep neural network-based reconstruction engine that is effective in reducing image noise while maintaining spatial resolution, texture, and sharpness in the brain, chest, and abdominal images based on previous clinical studies [8–10]. Furthermore, our study revealed that DLIR provided superior image quality for head and neck CT studies, which is consistent with the findings of earlier research.

The IR-based algorithm can reduce the radiation dose without degrading image quality compared with FBP, making it a routine choice for CT image reconstruction [11]. However, IR has its limitations such as diminished lesion detectability due to higher blending strength causing texture degradation [11]. DLIR, developed using deep neural networks and trained on high-dose FBP data, addresses these issues without sacrificing image quality [6]. However, IR has several limitations, which include decreased lesion detectability due to a higher blending strength leading to texture degradation [12]. DLIR, which was trained based on high-dose FBP data via the utilization of deep neural networks, overcomes such concerns without compromising image quality [7].

In clinical settings, three selectable strengths of DLIR with different denoise levels from low, medium, to high were used. Our study found that DLIR-M and DLIR-H produced the best image quality among all datasets, demonstrating statistically significant improvements in objective and subjective outcomes. Similar results have been reported in previous studies focusing on other body regions [9,10,13–17], including

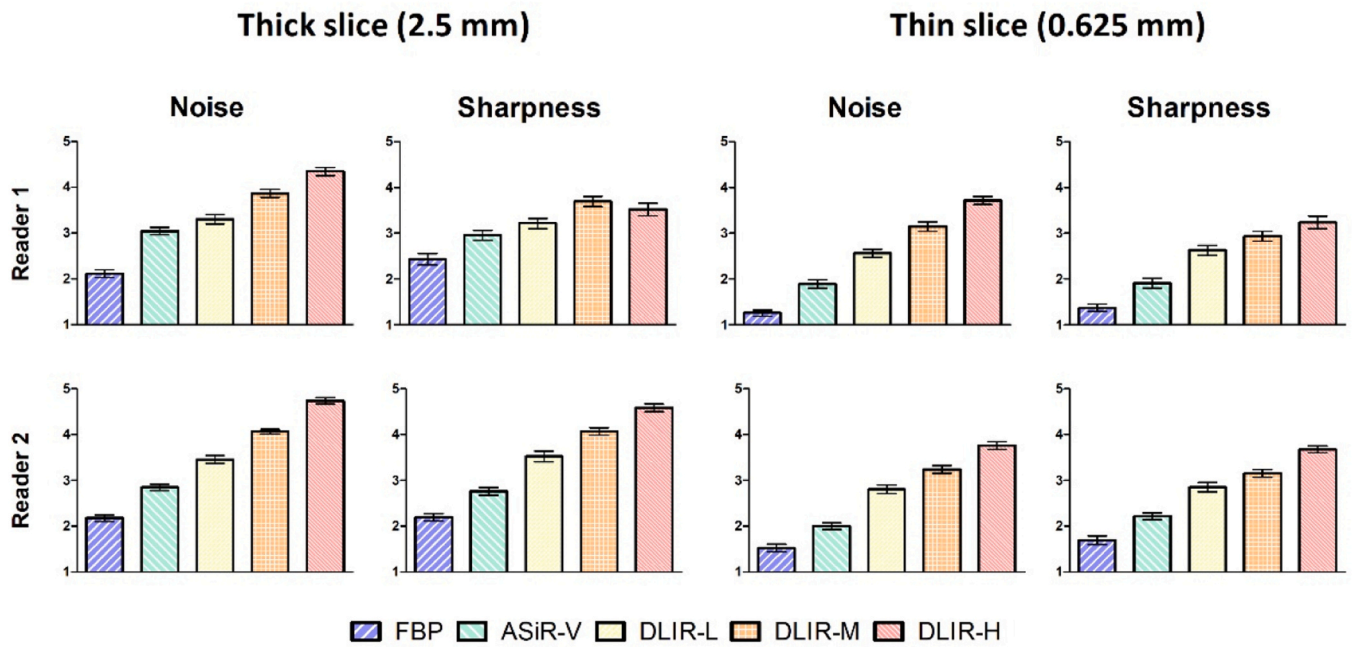


Fig. 4. Lymph node evaluation. Subjective score for sharpness and noise at 2.5-mm (a) and 0.625-mm (b) slice thickness provided by two readers.

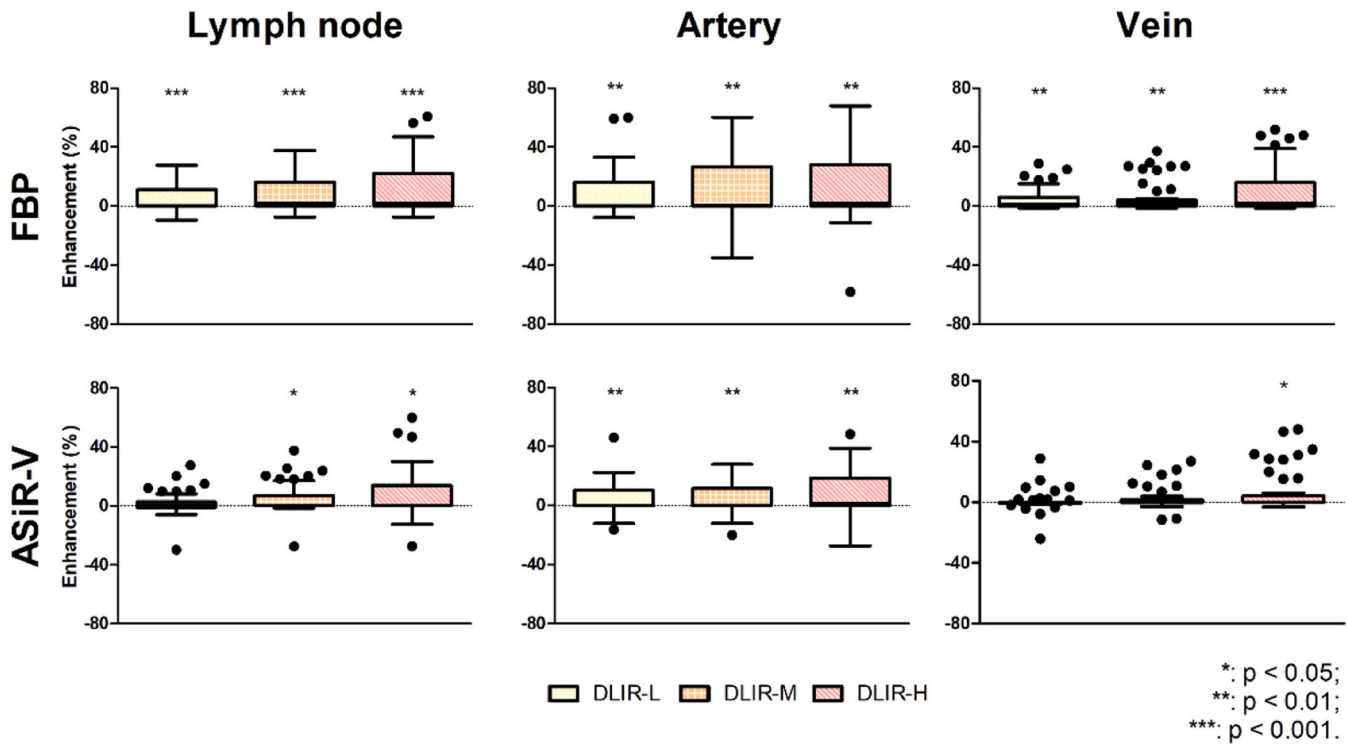


Fig. 5. Sharpness of the lymph nodes with peripheral arteries and veins between DLIR and FBP (upper row) and ASiR-V (lower row).

noncontrast-enhanced head CT images for trauma patients suspected of intracranial hemorrhage [16]. Further, Kim et al. revealed that images reconstructed with medium- and high-strength DLIR have a better image quality with reduced noise and artifacts [17]. Our findings are in line with those of prior research, indicating that DLIR holds significant potential as an advanced reconstruction method for diagnostic head and neck CT images.

In this study, we utilized images reconstructed with 0.625-mm slice

thickness to simulate reduced-dose protocol while maintaining diagnostic accuracy. DLIR consistently provided superior SNR and CNR values even with increased noise in thin-slice images. Moreover, medium- and high-strength DLIR demonstrated similar or better SNR and CNR than conventional reconstruction algorithms applied to thick-slice images. Sun et al. [9] showed that 0.625-mm thin-slice DLIR images enhanced lesion detection and produced comparable image noise to routine 5-mm ASiR-V images. The head and neck region contains

numerous small anatomically important structures, making thinner-slice images preferable for more precise diagnoses in CT images. Njølstad et al. found that DLIR achieved equal or superior abdominal image quality in 0.625-mm slices than in 2.5-mm slices using the standard ASiR-V algorithm [12]. Our findings suggest that DLIR can be effectively employed in reduced-dose protocols to decrease radiation exposure, particularly for pediatric and oncology patients who require frequent follow-up CT examinations. This has important clinical implications, as it enables more accurate diagnoses and monitoring while minimizing radiation exposure-associated potential risks.

In our clinical assessment, both readers were agreed that DLIR had superior quality for neck lymph node images and overall CT images based on visual scores. The ICC results indicated substantial agreement between readers when assessing image noise (ICC = 0.79) and reasonable agreement for artifact and image quality (ICC = 0.31 and 0.48, respectively). Jensen et al. reported that a reviewer observed minor blurring of extremely small lesions and vessels with high-strength DLIR [14]. Herein, the reader who awarded the highest rating for overall image quality and lymph node sharpness using DLIR-M made a similar observation. Another study also reported that increasing the strength of DLIR resulted in slightly blurred lesions measuring < 5 mm on abdominal CT images [18]. While studies have reported slightly blurred lesions with increased DLIR strength, others have revealed that high-strength DLIR yields the best visual scores and improved lesion conspicuity compared with different blending levels of ASiR-V [8,9,15,19]. This indicates that the overall benefits in terms of image quality and lesion detection can significantly contribute to more accurate diagnoses and treatment planning for patients while some minor trade-offs may exist with higher DLIR strengths.

In general, DLIR enhances the lesion visibility on diagnostic images for radiologists, particularly those of cervical lymph nodes that are often difficult to interpret due to adjacent metal implants. Since several studies only rely on visual assessment for evaluating sharpness, we employed FWHM to assess the margin of lymph nodes and peripheral vessels without reader bias. Most studies compared the sharpness between DLIR and ASiR-V rather than FBP; hence, we investigated differences in FWHM between DLIR and both reconstruction algorithms. DLIR-H and DLIR-M had superior performance in lymph nodes. However, there were no significant difference between DLIR-L and ASiR-V. These findings were in accordance with those of a previous study showing that DLIR had an unchanged or sharper peripancreatic vessel and common bile duct margins [8]. Additionally, higher ICCs of lymph node sharpness were demonstrated on thin-slice images compared with thick-slice images, indicating that reduced-dose protocol using DLIR can improve margin delineation. DLIR had a clearer morphological information on neck lymph nodes. Another study performed by the same team showed that with an increasing dose-reduction rate, the differences were more significant via visual assessment. This finding was in accordance with the results of this study [20]. In summary, the current study highlights significant improvements in the quality of cervical lymph node images on CT using medium- and high-strength DLIR.

We acknowledge the overarching importance of lymph node detectability and characterization in clinical practice while focusing on the comparison of the performance between different reconstruction algorithms in terms of image quality. The metrics evaluated in this study, such as noise reduction and edge sharpness, lay the groundwork for any subsequent clinical evaluations. We found no significant differences in lymph node sizes (5.21 ± 0.09 , $p = 0.66$) using these reconstruction algorithms, but we evaluated image-edge sharpness, which plays an essential role in the clinician's ability to accurately differentiate and characterize lymph nodes. Understanding these factors significantly enhances the diagnostic use of cervical CT scans. However, further research is required to directly assess the effects of these algorithms on lymph node detectability and characterization in various clinical scenarios.

This retrospective study had several limitations. First, it included a

relatively small sample size, and all data were collected from a single center. Second, there was sex bias that might require further investigation. Third, only the standard-dose protocol was used in this study, and the use of the reduced-dose protocol in clinical practice should be further evaluated. Additionally, additional readers are necessary to validate the diagnostic acceptability and confidence of precise clinical staging because this would help determine the clinical effect of our findings on patient management and outcomes. Furthermore, DECT-specific images were frequently used to assist diagnosis. The current study only demonstrated the results of 120-kVp-like images because 120-kVp-like images remain the primary choice for diagnosis. An investigation into image quality, specifically concerning low-keV images (at 60 keV) and iodine maps, was also conducted across all reconstruction algorithms for lymph nodes. These results have been appended to the [supplementary figure \(Supplementary Figure 1\)](#) and were closely aligned to 120-kVp-like images.

5. Conclusion

DLIR-M and DLIR-H outperformed conventional reconstruction algorithms in assessing the image quality of cervical lymph nodes on CT. In addition, thin-slice images reconstructed using DLIR-M and DLIR-H had similar quality to and better visual scores than thick-slice images reconstructed using FBP or ASiR-V. This advancement suggests that dose reduction can be implemented in clinical settings without sacrificing image quality in the future, ultimately enhancing the accuracy of cervical lymph node evaluations.

Funding statement

This study was financially supported by Ministry of Science and Technology of Taiwan. Grant numbers: MOST 111-2314-B-182A-037 and MOST 111-2314-B-182A-041.

Ethical statement

This retrospective study was approved by the Research Ethics Committee of Chang Medical Foundation (approval number: 2019019900B0). The requirement of informed consent was waived because of the retrospective nature of this study.

Declaration of Competing Interest

Author Ai-Chi Chen and Chia-Wei Lee were employed by General Electric (GE) Healthcare. The remaining authors declare no conflict of interest.

Appendix A. Supporting information

Supplementary data associated with this article can be found in the online version at [doi:10.1016/j.ejro.2023.100534](https://doi.org/10.1016/j.ejro.2023.100534).

References

- [1] P. Veit, et al., Lymph node staging with dual-modality PET/CT: enhancing the diagnostic accuracy in oncology, *Eur. J. Radio.* 58 (3) (2006) 383–389, <https://doi.org/10.1016/j.ejrad.2005.12.042>.
- [2] A. McErlean, et al., Intra- and interobserver variability in CT measurements in oncology, *Radiology* 269 (2) (2013) 451–459, <https://doi.org/10.1148/radiol.13122665>.
- [3] M.J. Willeminck, P.B. Noël, The evolution of image reconstruction for CT-from filtered back projection to artificial intelligence, *Eur. Radio.* 29 (5) (2019) 2185–2195, <https://doi.org/10.1007/s00330-018-5810-7>.
- [4] A. Mileto, et al., State of the art in abdominal CT: the limits of iterative reconstruction algorithms, *Radiology* 293 (3) (2019) 491–503, <https://doi.org/10.1148/radiol.2019191422>.
- [5] Z. Deák, et al., Filtered back projection, adaptive statistical iterative reconstruction, and a model-based iterative reconstruction in abdominal CT: an

- experimental clinical study, *Radiology* 266 (1) (2013) 197–206, <https://doi.org/10.1148/radiol.12112707>.
- [6] S. Notohamiprodjo, et al., Image quality of iterative reconstruction in cranial CT imaging: comparison of model-based iterative reconstruction (MBIR) and adaptive statistical iterative reconstruction (ASiR), *Eur. Radio.* 25 (1) (2015) 140–146, <https://doi.org/10.1007/s00330-014-3374-8>.
- [7] Jiang Hsieh, et al., A new era of image reconstruction: TrueFidelity™. White Paper, 2019.
- [8] P. Lyu, et al., Effect of deep learning image reconstruction in the prediction of resectability of pancreatic cancer: diagnostic performance and reader confidence, *Eur. J. Radio.* 141 (2021), 109825, <https://doi.org/10.1016/j.ejrad.2021.109825>.
- [9] J. Sun, et al., Application of a deep learning image reconstruction (DLIR) algorithm in head CT imaging for children to improve image quality and lesion detection, *BMC Med Imaging* 21 (1) (2021) 108, <https://doi.org/10.1186/s12880-021-00637-w>.
- [10] H. Yoon, et al., Image quality assessment of pediatric chest and abdomen CT by deep learning reconstruction, *BMC Med. Imaging* 21 (1) (2021) 146, <https://doi.org/10.1186/s12880-021-00677-2>.
- [11] Y. Nagayama, et al., Deep learning-based reconstruction for lower-dose pediatric CT: technical principles, image characteristics, and clinical implementations, *Radiographics* 41 (7) (2021) 1936–1953, <https://doi.org/10.1148/rg.2021210105>.
- [12] T. Njolstad, et al., Improved image quality in abdominal computed tomography reconstructed with a novel Deep Learning Image Reconstruction technique - initial clinical experience, 20584601211008391, *Acta Radio. Open* 10 (4) (2021), <https://doi.org/10.1177/20584601211008391>.
- [13] J.A. van Stiphout, et al., The effect of deep learning reconstruction on abdominal CT densitometry and image quality: a systematic review and meta-analysis, *Eur. Radio.* (2021), <https://doi.org/10.1007/s00330-021-08438-z>.
- [14] C.T. Jensen, et al., Image quality assessment of abdominal CT by use of new deep learning image reconstruction: initial experience, *AJR Am. J. Roentgenol.* 215 (1) (2020) 50–57, <https://doi.org/10.2214/ajr.19.22332>.
- [15] C. Park, et al., CT iterative vs deep learning reconstruction: comparison of noise and sharpness, *Eur. Radio.* 31 (5) (2021) 3156–3164, <https://doi.org/10.1007/s00330-020-07358-8>.
- [16] Z. Alagic, et al., Deep learning versus iterative image reconstruction algorithm for head CT in trauma, *Emerg. Radio.* 29 (2) (2022) 339–352, <https://doi.org/10.1007/s10140-021-02012-2>.
- [17] I. Kim, et al., Deep learning-based image reconstruction for brain CT: improved image quality compared with adaptive statistical iterative reconstruction-Veo (ASIR-V), *Neuroradiology* 63 (6) (2021) 905–912, <https://doi.org/10.1007/s00234-020-02574-x>.
- [18] T. Kaga, et al., Deep-learning-based image reconstruction in dynamic contrast-enhanced abdominal CT: image quality and lesion detection among reconstruction strength levels, *Clin. Radio.* 76 (9) (2021) 710.e15–710.e24, <https://doi.org/10.1016/j.crad.2021.03.010>.
- [19] A. Parakh, et al., Sinogram-based deep learning image reconstruction technique in abdominal CT: image quality considerations, *Eur. Radio.* 31 (11) (2021) 8342–8353, <https://doi.org/10.1007/s00330-021-07952-4>.
- [20] P. Lyu, et al., Is it possible to use low-dose deep learning reconstruction for the detection of liver metastases on CT routinely? *Eur. Radio.* (2022) <https://doi.org/10.1007/s00330-022-09206-3>.